Modeling of Microstructure Evolution, Residual Stresses and Distortions in 6082-T6 Aluminum Weldments

A process model for welding of age-hardening aluminum alloys has been developed

BY O. R. MYHR, S. KLOKKEHAUG, Ø. GRONG, H. G. FJÆR AND A. O. KLUKEN

ABSTRACT. This article illustrates the applications of process modeling for prediction of microstructure evolution, residual stresses and distortions in welding of hollow AA6082-T6 extrusions. The model consists of three components, *i.e.*, a numerical heat flow model, a microstructure model and a mechanical model that are sequentially coupled. It is shown that the model adequately predicts the temperature and local strength distribution. The calculated distortions were found to depend strongly on the welding sequence. Moreover, the local softening of the heat-affected zone was shown to have a significant effect on the simulated residual stress distribution.

Introduction

Weldments are prime examples of components where the properties achieved depend upon the characteristics of the microstructure. This description applies in particular to structural parts of age hardening aluminum alloys, which are being used with increasing frequency in the transport and automotive industry because of their high strength, good formability, low density and good resistance to general corrosion. In certain cases, the application of aluminum is restricted by a low heat-affected zone (HAZ) strength level due to softening reactions occurring during welding. In other cases, cracking resistance, fatigue strength or global distortion becomes the limiting factor, depending on the design criterion.

In recent years, significant progress has been made in the understanding of physical processes that take place during welding of aluminum alloys. A synthesis of that knowledge has, in turn, been consolidated into process models, which provide a mathematical description of the relation between the main welding variables (*e.g.*, heat input, plate thickness, joint configuration, etc.) and the subsequent weld properties, based on sound physical principles (Refs. 1–8). The components of such a model will be

1) A heat flow model for prediction of the temperature-time pattern during welding

2) Kinetic models for prediction of the HAZ microstructure evolution (*e.g.*, volume fraction of hardening precipitates) as a function of temperature

3) Constitutive equations, based on dislocation or continuum mechanics, which can be implemented into FE codes and provide quantitative information about the resulting heat-affected zone (HAZ) properties such as strength or residual stress level

In the present investigation the concept is further developed and applied to modeling of the relation between heat flow, microstructure evolution, residual stresses and distortions during welding of hollow 6082-T6 extrusions. As a starting point, a general framework for handling complex problems of this kind is presented, based on the internal state variable approach. Here, the basic idea is to capture the microstructure evolution and deformation fields in terms of differential variations of some state variables with time for each of the relevant mechanisms. Separate response equations are then developed to convert the current values of the stated variables into measurable quantities such as hardness, yield strength and accumulated stresses or strains. The outputs from the model will be illustrated in different numerical examples and case studies.

O. R. MYHR and A. O. KLUKEN are with the Hydro Raufoss Automotive Research Centre, Raufoss, Norway; H. G. FJÆR and S. KLOKKEHAUG are with the Institute for Energy Technology, Kjeller, Norway; and Ø. GRONG is with the Department of Metallurgy at the Norwegian University of Science and Technology, Trondheim, Norway.

KEY WORDS

Welding
Modeling
Simulation
Microstructure
HAZ Softening
Residual Stresses
Distortions
Aluminum Alloys

Components of Model

The process model consists of three components that are sequentially coupled, *i.e.*, a numerical heat flow model, a microstructure model and a mechanical model. The coupling between the different models is shown in Fig. 1. According to the assumptions, the imposed temperature field influences both the microstructure evolution and the stress deformation field. At the same time, there is a link between the microstructure model and the mechanical model to take into account the important effect of heat-affected zone softening on the strain relaxation during cooling. In practice, this occurs by local yielding within the high peak temperature regions of the HAZ.

Problem Description

Figure 2 summarizes the important metallurgical reactions to be modeled during welding of 6082-T6 aluminum alloys. It is evident from Fig. 2A that reversion of β″-precipitates will occur to an increasing extent in the peak temperature range from 220–500°C (428–932°F). This is associated with a continuous decrease

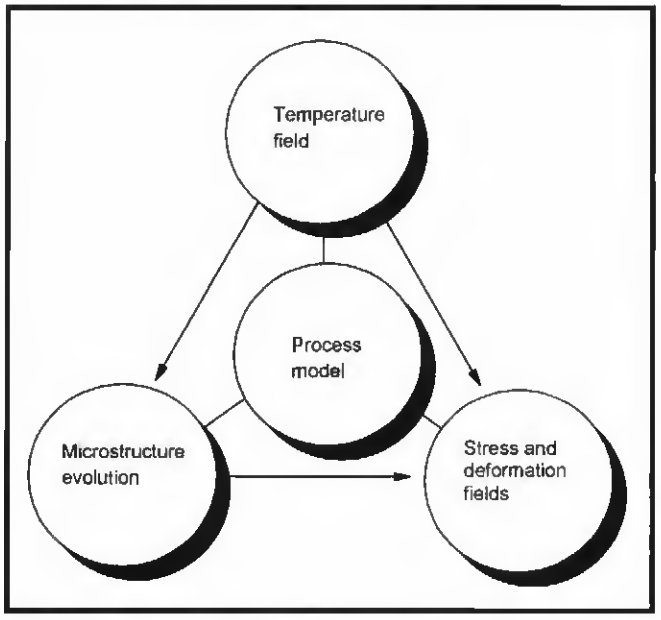

Fig. 1 — Schematic diagram illustrating the coupling between the different submodels.

Table 1 — Summary of Input Data Used in Computer Simulations

Parameter	Value	Comments
A_0	3.6×10^8 JK^{-2} mol^{-1}	From Ref. 4
HV_{max}	110	Measured
HV_{min}	42	Measured
Q_d	130 kJ/mol	From Ref. 4
Q_s	30 kJ/mol	From Ref. 4
T_c	673 K	From Ref. 12
T_{r1}	648 K	Chosen
T_{r2}	623 K	Chosen
T_s	793 K	From Ref. 4
t_{r1}	200 s	Calibration parameter
t_{r2}	3 s	Calibration parameter
Ψ	0.56	From Ref. 4

Table 2 — Composition of Aluminum Alloy 6082-T6 (wt-%)

Element	Si	Mn	Mg	Fe	Cr	Cu	Ti	Al
Content	0.82	0.59	0.56	0.20	0.17	0.01	0.01	bal.

in the HAZ hardness until the dissolution process is completed. During cooling of the weld, some solute recombines to form coarse, metastable β'(Mg_2Si) precipitates that do not contribute to strengthening — Fig. 2B. However, close to the fusion boundary, a large fraction of alloying elements will remain in solid solution at the end of the thermal cycle, thereby giving conditions for extensive age hardening at room temperature over a period of 5 to 7 days — Fig. 2C.

Heat Flow Model

The numerical code is based on the computer program ALSIM (Ref. 9). Briefly, the program solves the three-dimensional, time-dependent heat conduction equation by a finite element technique.

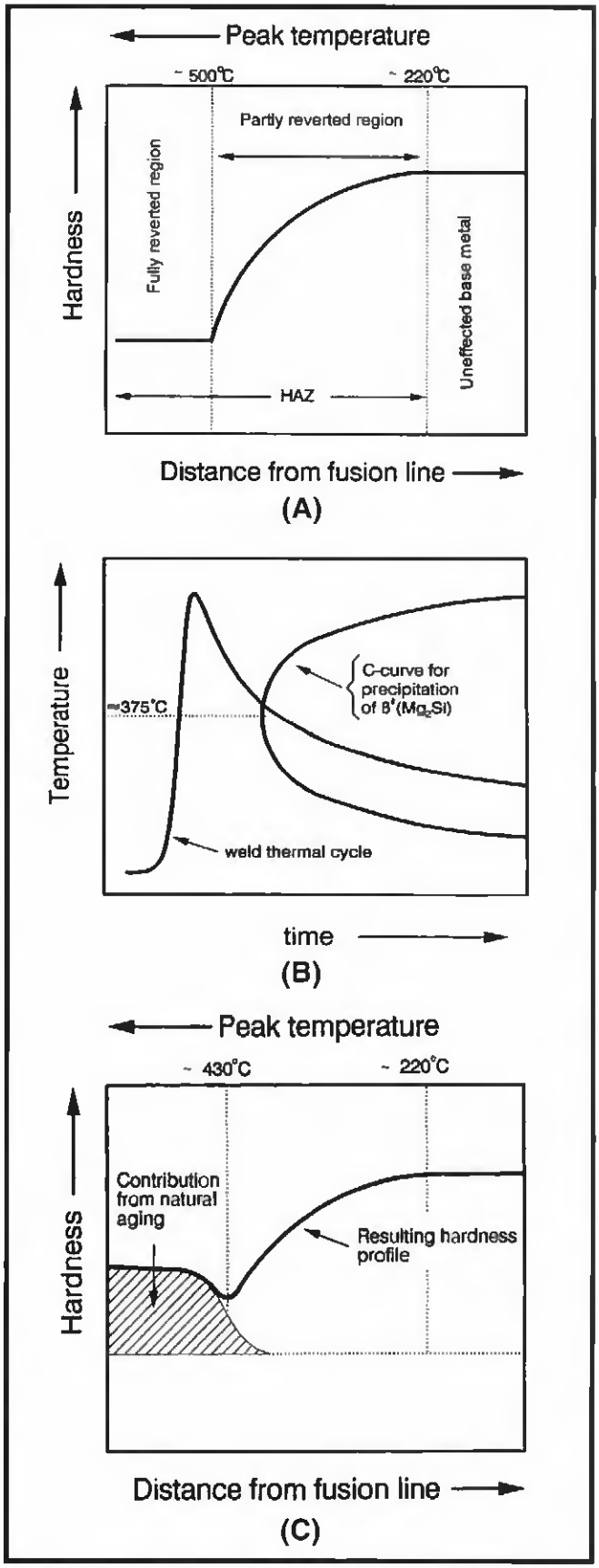

Fig. 2 — Schematic diagrams showing the sequence of reactions occurring in the HAZ of 6082-T6 aluminum alloys; A — hardness distribution following β"(Mg_2Si) dissolution; B — precipitation of β'(Mg_2Si) during the weld cooling cycle; C — hardness distribution following prolonged room temperature aging.

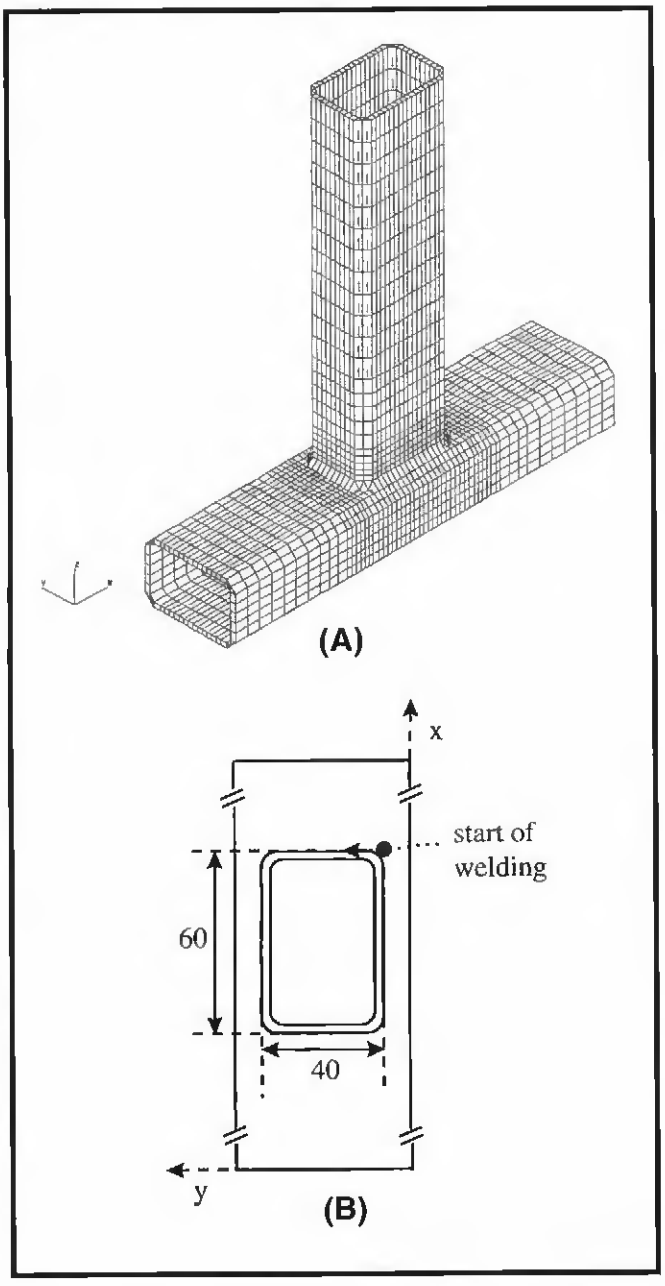

Fig. 3 — Geometry of hollow extrusion profile; A — details of element mesh; B — cross section at the upper horizontal surface of the extrusion at z = 0 showing the start position of the weld. (All dimensions in mm.)

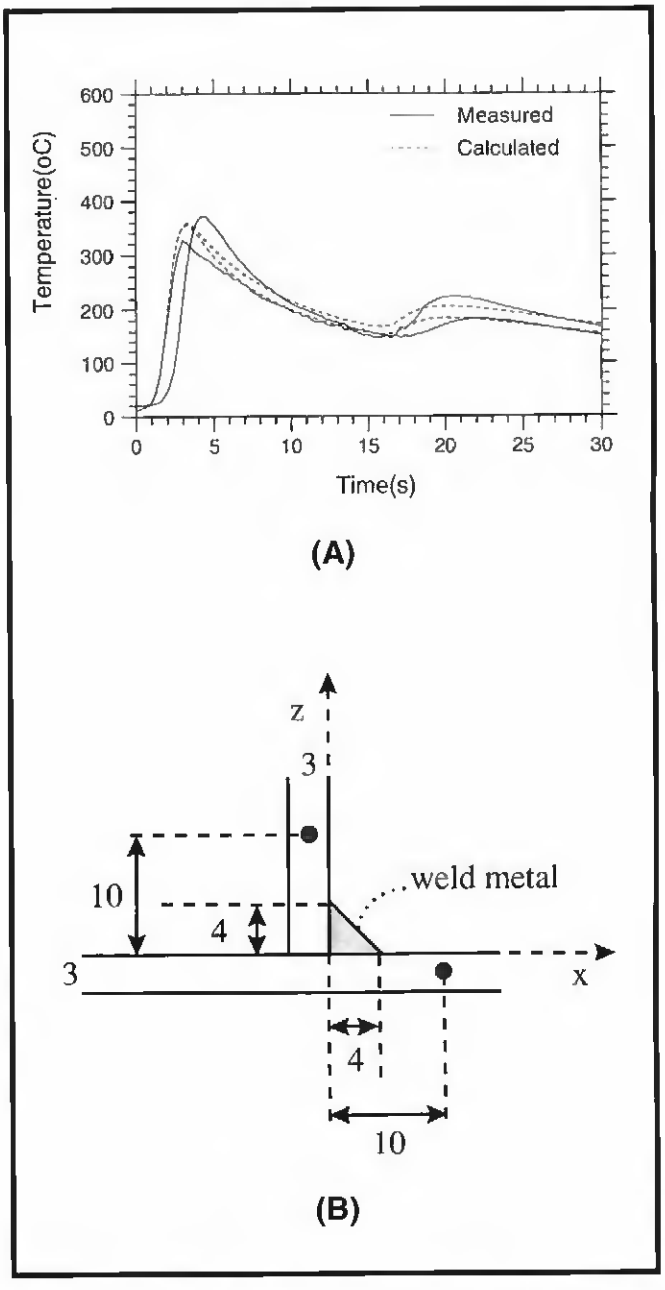

Fig. 4 — Comparison between measured and predicted weld thermal cycles at two different locations. (All dimensions in mm.) A — Temperature-time pattern; B — positions of thermocouples within the hollow tube.

The latent heat of fusion is included in the specific heat function between the solidus and liquidus temperatures, allowing alloys with a freezing range to be simulated. The heat released by the welding arc is represented by an ellipsoid volume distributed source, where the heat distribution is calibrated against measurements of the weld pool geometry. To account for the metal deposition from the consumable electrode, elements that are part of the weld reinforcement are continuously activated during welding at material points that coincide with the instantaneous position of the moving heat source. The boundary conditions are represented by heat transfer coefficients between the material and the environment. The calculated temperature-time history for each material point is used as an input to a separate subroutine that calculates the corresponding fraction of hardening precipitates at each time step.

Microstructure Models

The microstructure models provide a mathematical description of the reaction sequence outlined in Fig. 2. Here, we summarize the main features of the models (details have been reported elsewhere — Refs. 1, 4, 6, 8, 10).

Reversion Model

If the number of particles per unit volume is constant, and the particle volume fraction f and radius r do not vary independently, reversion can be described by a single state variable f. Under such conditions simple diffusion theory shows that the volume fraction falls from its

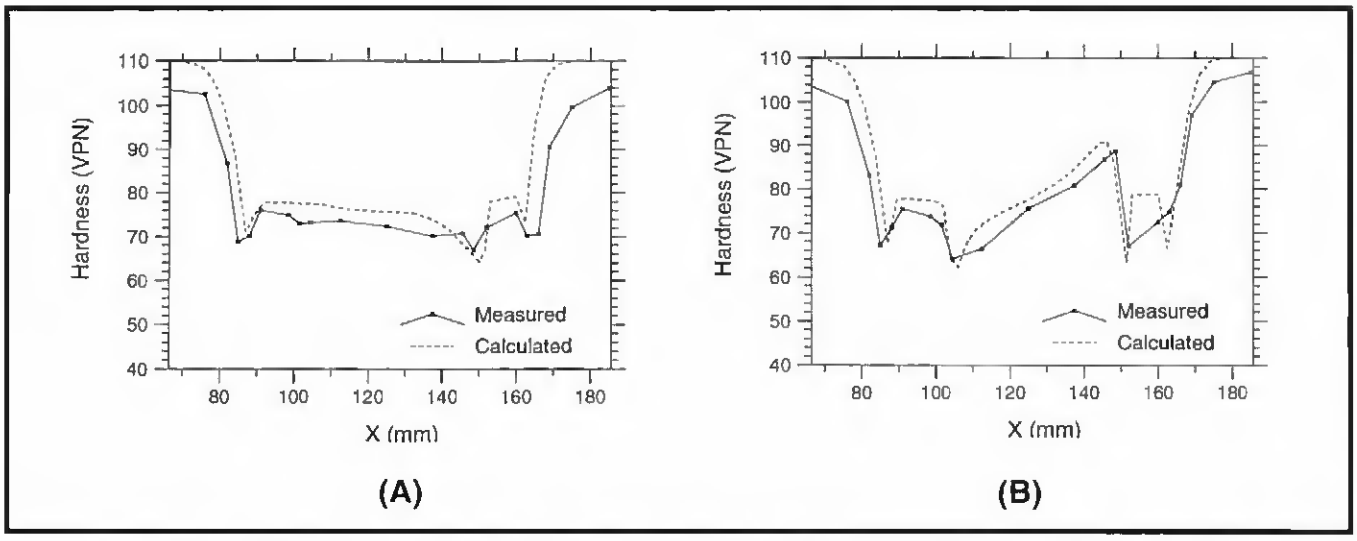

Fig. 5 — Comparison between measured and predicted HAZ hardness profiles in different positions across the upper horizontal surface of the hollow extrusion; A — along the x-axis at y =18.5 mm and z = 0; B — along the x-axis at y =30 mm and z = 0.

initial value f_0 according to the equation (Refs. 4, 8)

$$f / f_0 = 1 - \left[\int dt / t_1^*\right]^{n_1} \quad (1)$$

where n_1 is a time exponent (< 0.5), and t_1^* is the time taken for complete particle dissolution at a given temperature, defined as (Refs. 4, 8)

$$t_1^* = t_{r1} \exp\left[\left(\frac{Q_s}{n_1 R} + \frac{Q_d}{R}\right)\left(\frac{1}{T} - \frac{1}{T_{r1}}\right)\right] \quad (2)$$

In Equation (2), t_{r1} denotes the time for complete particle dissolution at a chosen reference temperature T_{r1}. Q_s is the metastable solvus boundary enthalpy, Q_d is the activation energy for diffusion of the less mobile constitutive atom of the precipitates and R is the universal gas constant. Because Equation (1) satisfies the additivity conditions pertaining to an isokinetic reaction, it can be integrated numerically over the actual weld thermal cycle in any position within the HAZ.

Natural Aging Model

By considering the form of the C curve for precipitation of nonhardening β'-(Mg_2Si) precipitates at dispersoids, and the subsequent natural aging kinetics, Myhr and Grong (Ref. 4) arrived at the following expression for the net precipitation increment, referred to the initial content of hardening phases in the peak aged base material:

$$f^* / f_0 = \Psi\left[\left(1 - X_C\right)^{I_1} - \alpha_1\right]^2 \quad (3)$$

where

$$I_1 = \left[\int dt / t_2^*\right]^{n_2}. \quad (4)$$

In Equation (3) α_1 is a dimensionless strength parameter defined in Equation (6), while Ψ is a proportionality constant. t^*_2 denotes the time taken to precipitate a certain fraction ($X = X_C$) of β' at an arbitrary temperature, T. The variation of t^*_2 with temperature is given by (Refs. 4, 10)

$$t_2^* = t_{r2} \exp\left\{\frac{A_0}{R}\left[\frac{1}{T\left(T_s - T\right)^2} - \frac{1}{T_{r2}\left(T_s - T_{r2}\right)^2}\right] + \frac{Q_d}{R}\left(\frac{1}{T} - \frac{1}{T_{r2}}\right)\right\} \quad (5)$$

where t_{r2} is the critical hold time required to precipitate a certain fraction of β'-Mg_2Si at a chosen reference temperature T_{r2}. T_s is the phase boundary solvus temperature, and A_0 is a material constant related to the nucleation potency of the dispersoids with respect to β'-Mg_2Si.

Response Equations

The strength of 6XXX alloys is primarily determined by the density and size of the hardening β"-(Mg_2Si) precipitates. When the β"-particles dissolve, the volume fraction falls from its initial value f_0 according to Equation (1). The resulting change in the local strength level is calculated via the following response equation, which can be obtained from simple dislocation theory (Refs. 1, 4):

$$\alpha_1 = \left(HV - HV_{\min}\right) / \left(HV_{\max} - HV_{\min}\right) = f / f_0 \quad (6)$$

where HV_{min} is the intrinsic matrix strength after complete particle dissolution, while HV_{max} is the original base metal strength for the actual temper condition (e.g., artificially aged (T6) or naturally aged (T4) material).

Similarly, Equation (3) yields the volume fraction of hardening precipitates that form during natural aging (f^*). After 5–7 days natural aging, the corresponding net strength increment (α_2) can be written as

$$\alpha_2 = f^* / f_0 = \left(HV - HV_{\min}\right) / \left(HV_{\max} - HV_{\min}\right) \quad (7)$$

Coupling of Reversion and Aging Models

Based on Equations (1) through (7), it is possible to calculate the HAZ strength distribution after welding and subsequent natural aging when the weld thermal program is known. Since the resulting strength level in the partly reverted region depends on the interplay between two competing processes (*i.e.*, dissolution and reprecipitation), it is convenient to define the "boundary" between the models on the basis of the intersection point, where $\alpha_1 = \alpha_2$, *i.e.*:

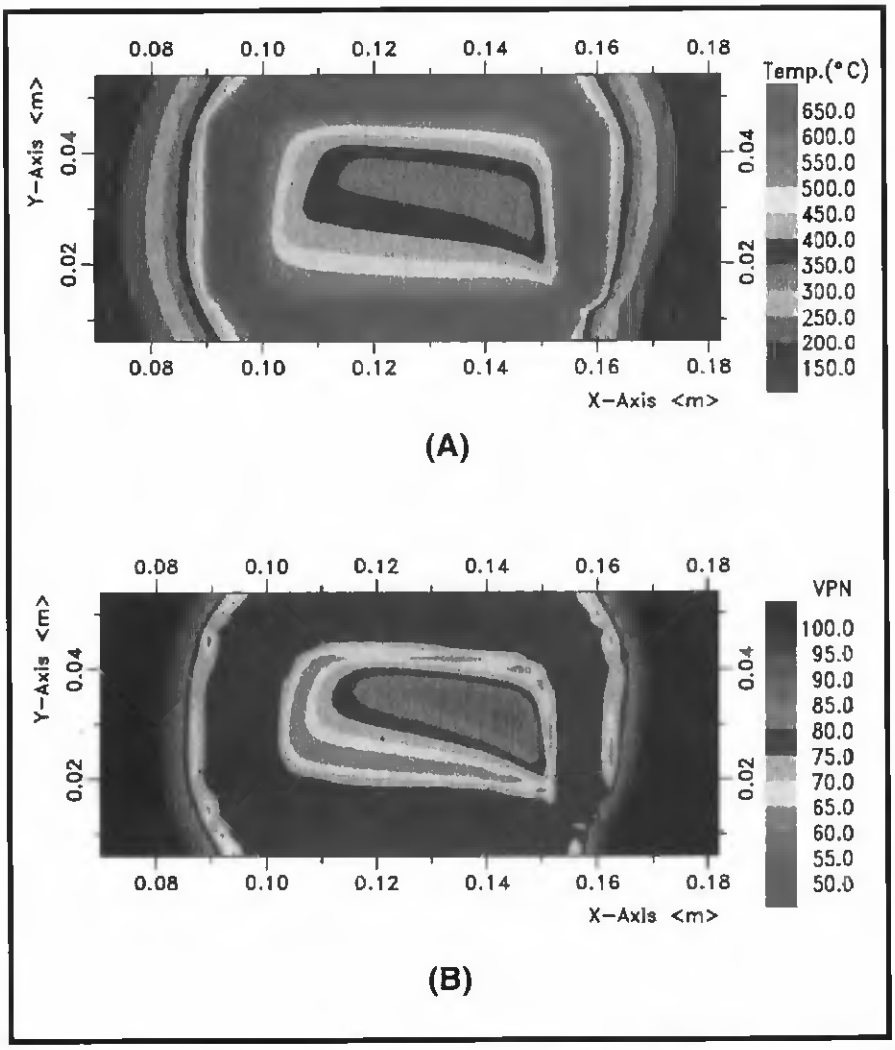

Fig. 6 — Examples of outputs from thermal and microstructure models; A — peak temperature distribution across the upper horizontal surface of the hollow extrusion (temperatures in °C); B — resulting HAZ hardness contours after prolonged room temperature aging (hardness in VHN).

$$HV = HV_{\min} + (HV_{\max} - HV_{\min})\alpha_1 \quad \text{when } \alpha_1 \geq \alpha_2; \tag{8}$$

$$HV = HV_{\min} + (HV_{\max} - HV_{\min})\alpha_2 \quad \text{when } \alpha_2 > \alpha_1. \tag{9}$$

It follows that this locus also defines the minimum HAZ strength level, which is an important parameter in engineering design.

Mechanical Model

In the present investigation, a special numerical code, originally developed for prediction of strains and stresses during direct chill (DC) casting of aluminium (Refs. 11, 12), has been adopted for the weld simulation with minor modifications. The model assumes isotropic elastic-viscoplastic behavior where the well known Prandtl-Reuss relations are applied to calculate the viscoplastic strain increments.

The relationship between flow stress σ, temperature T, the strain hardening parameter ϕ and the effective viscoplastic strain rate $\dot{\varepsilon}_p$ is given by the following response equation (Ref. 12), which in the present case has been modified to incorporate the effect of microstructure evolution via a separate $A(f/f_0)$ term:

$$\sigma = A(f/f_0)F(T)(\phi + \phi_0)^{n(T)}(\dot{\varepsilon}_p)^{m(T)}.$$

If the temperature is below a certain critical value, T_c, the evolution of the hardening parameter is calculated from viscoplastic strain increments as follows:

$$d\phi = d\varepsilon_p. \tag{11}$$

Similarly, at higher temperatures, we have

$$d\phi = 0. \tag{12}$$

The assumption of pure creep above T_c is based on experience with a similar alloy in the as-cast condition (Ref. 13). Equation (10) provides an adequate description of the true stress-strain behavior within the HAZ during welding. However, since this relation is empirical and based on a limited amount of experimental data, attempts are currently being made to obtain a sounder physical basis for the microstructure coupling.

Note the mechanical model does not include a consideration of the liquid metal pool. This means that each element in the weld pool first becomes mechanically activated when the temperature drops below the dendrite coherency temperature of the material.

Numerical Examples and Case Studies

The dissolution, aging and mechanical models have been implemented in a dedicated FE code for prediction of the HAZ hardness distribution and the resulting stress-strain response. The calculated temperature-time history for each material point is used as an input to a separate subroutine that calculates the corresponding fraction of hardening precipitates, f, at each time step. The state variable f is, in turn, input to the mechanical model, which calculates the stress and strain evolution. The different input data used in the simulations are summarized in Table 1.

Experimental Program

As an illustration of principles, the process model is applied to welding of a structural component for automotive applications. The component consists of two identical rectangular tubes of the alloy AA6082-T6 with composition as shown in Table 2. The dimensions are 60 x 40 mm with 3-mm wall thickness, where the butt end of one tube is welded against the flat side of the other using fully automatic GMA-welding — Fig. 3A. The weld deposition was carried out along the circumference of the tube in one pass at a constant speed of 12 mm/s, as shown in Fig. 3B. The net arc power was kept constant and equal to 2.38 kW for the first half of the weld (assuming an arc efficiency of 0.78) and was then reduced to 2.24 kW for the remaining part of the weld to avoid full penetration. The thermal model was validated by comparison with *in situ* ther-

mocouple measurements. Moreover, a series of hardness measurements was carried out across the weld HAZ after seven days of room temperature aging to check the accuracy of the microstructure model. The hardness impressions within the vertical tube walls were done after the tube had been sectioned along the circumference of the weld.

Temperature and Hardness Distribution

Figure 4 shows a comparison between calculated and measured thermal cycles at different positions within the HAZ. It is evident that the numerical heat-flow model adequately predicts the HAZ temperature-time pattern, including the secondary reheating that takes place due to overlap of temperature fields from different weld regions.

Figure 5 shows a comparison between predicted and measured hardness values in different surface positions of the horizontal tube. In general, the predictive power of the model is good, and it is also able to reproduce the observed asymmetry in the hardness distribution resulting from a corresponding asymmetry in the temperature distribution. The important effect of heat-flow conditions is further illustrated in Fig. 6, which shows plots of the peak temperature distribution and the corresponding hardness contours across the upper horizontal surface of the weld HAZ.

Residual Stresses and Distortions

In addition to the real welding situation (case A) described above, two other simulations were carried out. In the second simulation (case B), the welding sequence was changed. In a third simulation (case C), the mechanical model was fully decoupled from the microstructure model by omitting the term $A(f/f_0)$ from the equation governing the viscoplastic flow (*i.e.*, Equation 10). Under such conditions, the flow stress will be a unique function of temperature for fixed values of ε and ϕ, as shown in Fig. 7.

Figure 8A, B and C show the calculated normal stress component along the tube axis (*i.e.*, xx-component) of the residual stresses near the upper surface of the horizontal tube. As can be seen, the stress distribution is strongly dependent on the welding sequence. At the same time, much higher residual stresses are generated if the HAZ softening due to particle dissolution is neglected in the calculations. This observation is not surprising, considering the important effect of matrix yielding on the stress relaxation.

A similar dependency on welding sequence and microstructure evolution is

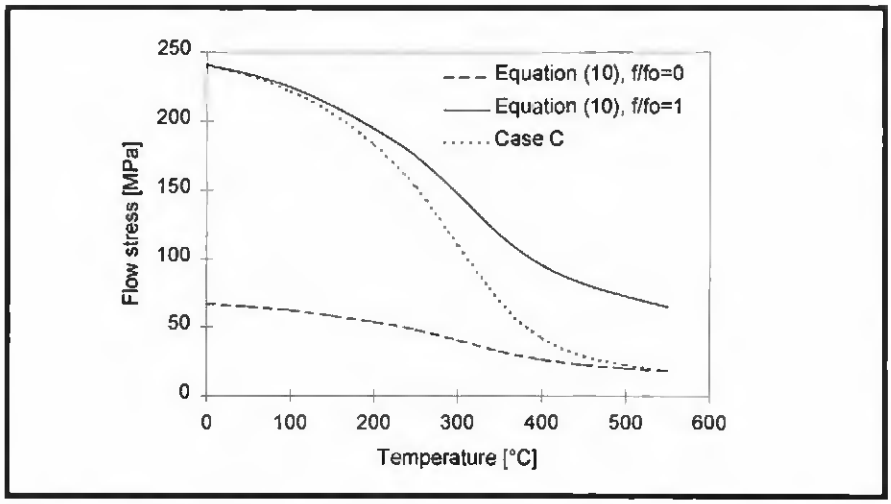

Fig. 7 — Graphical representation of the flow stress as a function of temperature for constant values of strain rate ($\dot{\varepsilon} = 10^{-3}\ s^{-1}$) and the strain hardening parameter ($\phi = 0$). The solid lines represent the extreme cases where $f/f_0 = 0$ and 1, respectively in Eq. (10). The broken line represents Case C where the flow stress is a unique function of temperature.

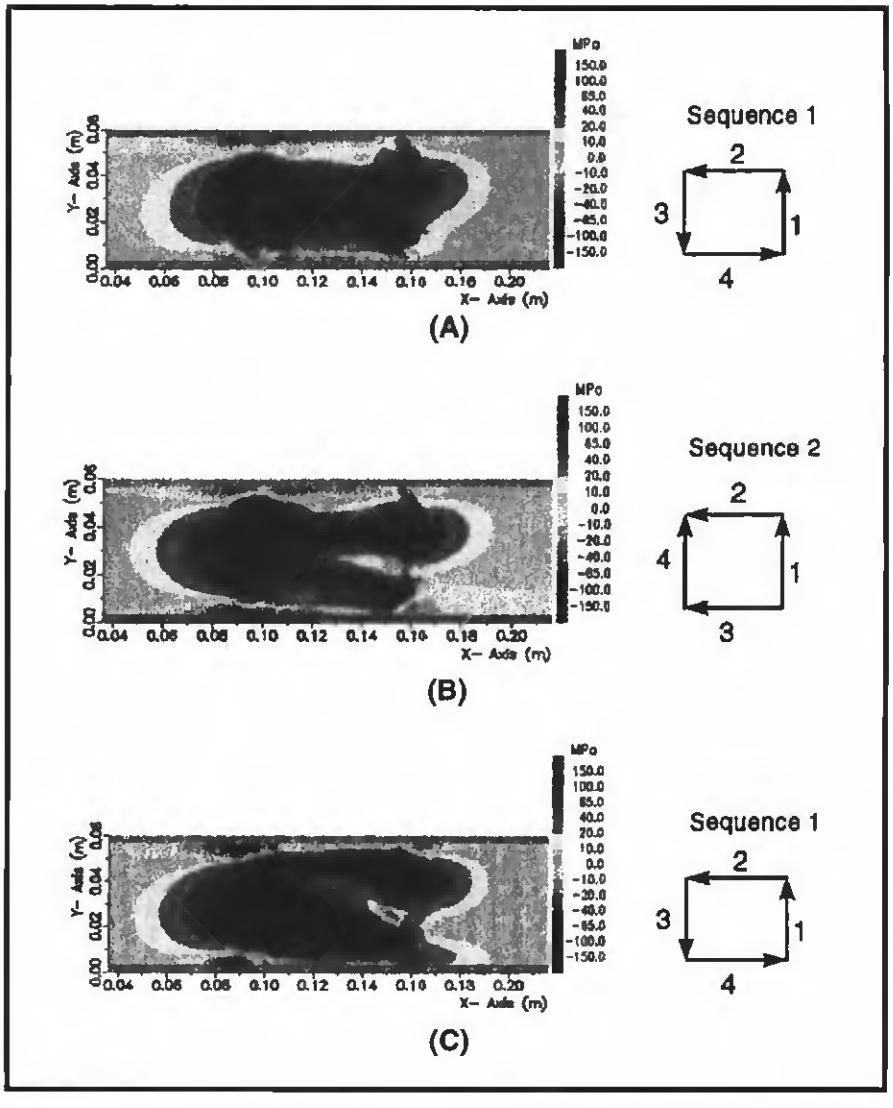

Fig. 8 — Calculated xx components of the residual stresses near the upper surface of the horizontal tube. A — Case A; B — case B; C — case C.

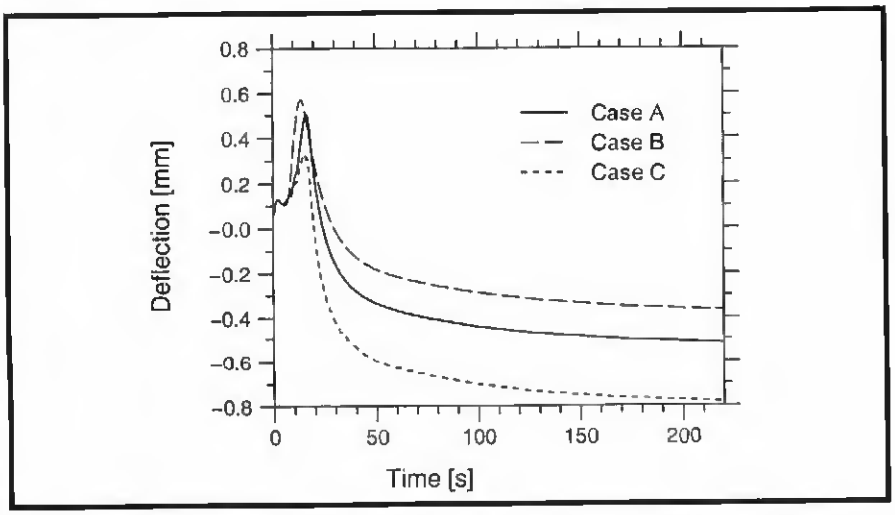

Fig. 9 — Calculated vertical deflections at the center of the side wall of the horizontal tube as a function of time.

shown in Fig. 9 for the global distortions at the center of the side wall of the horizontal tube. These results are interesting from both an academic and practical point of view since they illustrate in a quantitative manner how process modeling can be used as a tool to minimize damage caused by welding.

Conclusions

The basic conclusions that can be drawn from the present work are the following:

1) A process model for welding of age hardening aluminium alloys has been developed. The model consists of three components, *i.e.*, a numerical heat flow model, a microstructure model and a mechanical model that are sequentially coupled.

2) In general, the microstructure evolution and the deformation fields can be captured mathematically in terms of differential variations of some state variables with time for each of the relevant mechanisms. Separate response equations are then developed to convert the current values of the state variables into measurable quantities, such as hardness, yield strength and accumulated stress or strain.

3) By implementing the different components of the model in a dedicated FE code, welding of complex geometries (e.g., hollow extrusions and T-joints) can be simulated. A comparison between theory and experiments shows the process model adequately predicts both the HAZ temperature and strength distribution.

4) Indications are that local softening occurring during welding has a significant effect on the resulting residual stress field and global distortions. Consequently, to improve the confidence in the simulations, due consideration should be given to the HAZ microstructure evolution.

Acknowledgments

The authors wish to acknowledge the financial support of Hydro Aluminium and The Research Council of Norway.

References

1. Grong, O. 1997. *Metallurgical Modelling of Welding*, 2nd ed., The Institute of Materials, London.

2. Shercliff, H. R., and Ashby, M. F. 1990. *Acta Metall. Mater.*, no. 38, 1789–1802, 1803–1812.

3. Sarrazin, E. 1995. Ph.D. thesis, Ecole Polytechnique, Palaiseau, France.

4. Myhr, O. R., and Grong, Ø. 1991. *Acta Metall. Mater.*, no. 39, 2693–2702, 2703–2708.

5. Shercliff, H. R., Grong, Ø., Myhr, O. R., and Ashby, M. F. 1992. Proc. The 3rd International Conf. on Aluminium Alloys (ICAA3), Vol. III, 357–369, Trondheim.

6. Grong, Ø., and Myhr, O. R. 1993. *Mathematical modelling of weld phenomena*, eds. H. Cerjak and K. E. Easterling, The Institute of Materials, London, pp. 300–311.

7. Midling, O. T., and Grong, Ø. 1994. Acta metall. mater., 42, 1595–1609; 1611–1622.

8. Myhr, O. R., Grong, Ø., Klokkehaug, S., Fjær, H. G., and Kluken, A. O. 1997. *Science and Technology of Welding and Joining* 2(6): 245–254.

9. Håkonsen, A., and Mortensen, D. 1995. Modelling of casting, welding and advanced solidification processes VII, Warrendale, Pa. TMS-AIME, pp. 963–970.

10. Bratland, D. H., Grong, O., Shercliff, H. R., Myhr, O. R., and Tjøtta, S. 1997. Overview No. 124, *Acta mater*, 45, 1–22.

11. Fjær, H. G., and Jensen, E. K. 1995. Light Metals, TMS, pp. 951–959.

12. Fjær, H. G., and Mo, A. 1990. *Met. Trans.* 21B, pp. 1049–1061.

13. Nedreberg, M. L. 1991. Ph.D. thesis, University of Oslo, Oslo, Norway.

List of Symbols

A	Dimensionless function in mechanical model.
A_0	Material constant for nucleation of β'-(Mg^2Si) in aluminium (J/K^2mol).
α_1, α_2	Dimensionless strength parameters.
ε_p	Effective viscoplastic strain.
$\dot{\varepsilon}_p$	Effective viscoplastic strain rate (1/s).
F	Temperature dependent function in mechanical model (MPa).
f	Volume fraction of precipitates.
f_0	Initial volume fraction of precipitates.
f^*	Volume fraction of hardening precipitates in natural aging model.
ϕ	Strain hardening parameter in mechanical model.
ϕ_0	Initial value of strain hardening parameter.
HV	Hardness (VHN).
HV_{max}	Base metal hardness (VHN).
HV_{min}	Intrinsic matrix hardness in absence of hardening precipitates (VHN).
h	Heat transfer coefficient between workpiece and backing plate (W/m^2K).
I_1	Kinetic strength of thermal cycle with respect to β' precipitation.
m, n	Temperature dependent exponents in mechanical model.
Q_d	Activation energy for diffusion (J/mol).
Q_s	Solvus boundary enthalpy (J/mol).
R	Universal gas constant (8,314 J/mol K).
t	Time (s).
t_1^*	Time taken to dissolve a certain fraction of the precipitates at an arbitrary temperature (s).
t_2^*	Time taken to precipitate a certain fraction of β'-particles at an arbitrary temperature.
t_{r1}	Time for complete particle dissolution at T_r in dissolution model (s).
t_{r2}	Critical hold time required to precipitate a certain fraction of β' (Mg_2Si) at T_r (s).
T	Temperature (K).
T_C	Critical temperature for strain hardening (K).
T_{r1}	Chosen reference temperature for dissolution of $\beta''(Mg_2Si)$ (K).
T_{r2}	Chosen reference temperature for precipitation of $\beta'(Mg_2Si)$ (K).
T_s	Phase boundary solvus temperature (K).
X_C	Fraction $\beta'(Mg_2Si)$ precipitated during t_{r2} at the temperature T_{r2}.
Ψ	Material constant in aging model.